Supplementary Information

Gas medium annealing for perovskite solar cells with the state-of-the-art energy loss

Mengjiong Chen,[a] Zhenzhen Qin,[a] Ziyang Zhang,[a] Yanbo Wang,*[a] and Liyuan Han*[a]

[a] State Key Laboratory of Metal Matrix Composites, Shanghai Jiao Tong University, 800 Dong Chuan Road, Shanghai 200240, China. Email: sjtu-wyb@sjtu.edu.cn, han.liyuan@sjtu.edu.cn.

Materials

Nickel acetylacetonate was purchased from Adamas. Acetonitrile, ethanol absolute, dimethylformamide (DMF), dimethyl sulfoxide (DMSO), 2-propanol (IPA) and chlorobenzene (CB) were purchased from Sigma Aldrich. (4-(3,6-dimethyl-9H-carbazole-9-yl) butyl) phosphonic acid (Me-4PACz), lead iodide (PbI_2), formamidinium iodide (FAI), cesium iodide (CsI), phenylethylamine chloride (PEACl), tin(II) iodide (SnI_2), methylammonium iodide (MAI) and ammonium thiocyanate (NH_4SCN) were purchased from Tokyo Chemical Industry. Methylammonium chloride (MACl) and bathocuproine (BCP) were purchased from Xi' an Yuri Solar Co., Ltd. Ammonium dithiocarbamate (AMD) and tin(II) fluoride (SnF_2) were purchased from Shanghai Aladdin Biochemical Technology. PCBM was purchased from Luminescence technology corp. All the chemicals are used directly without further purification.

Normal bandgap PSCs fabrication

F-doped SnO_2 (FTO) glass substrate was cleaned by sequentially washing with detergent, deionized water, ethanol absolute, acetone, and isopropanol. Before use, the FTO was cleaned with ultraviolet ozone for 20 minutes. NiO films were prepared by spray pyrolysis in air, which were synthesized similarly to previous reports.[1] Then the substrates were transferred to a N_2 filled glove box while the substrate is still hot. 1.0 mg/ml Me-4PACz dissolved in ethanol absolute was deposited on the NiO films at 4000 rpm for 30 seconds, followed by annealing at 100 ^oC for 10 minutes. For deposition of perovskite layer, 1.4 M perovskite precursor solution was prepared by mixing CsI, FAI and PbI_2 in DMF : DMSO (4:1/v:v) mixed solvents with a chemical formula of $Cs_{0.05}FA_{0.95}PbI_3$, 5 mol% of excess PbI_2 was needed to improve the device performance. Then, 12 mol% MACl was added to the perovskite precursor solution and stirred for 2 hours. 120 μL perovskite solution was dripped on the substrate, followed by a two-step spin-coating of 1000 rpm for 12 seconds and 5000 rpm for 38 seconds. 150 μL CB was dripped onto the center of film at 12 seconds before the end of spin-coating. The

perovskite intermediate phase was subsequently annealed on a hotplate at 100 ºC for 20 minutes. As for GMA-perovskite films, 1 g AMD powder was placed on the hot plate 2 minutes in advance to create the annealing atmosphere. The entire process involves covering AMD powder and perovskite films with a 10 cm diameter culture dish. As for NH_3-perovskite films, NH_3 was introduced at a rate of 0.5 L/min for 30 seconds prior to annealing to create the annealing atmosphere and the same rate was maintained throughout the entire process. As for CS_2-perovskite films, 200 μL CS_2 was placed on the hot plate 30 seconds in advance to create the annealing atmosphere. The entire process involves covering CS_2 and perovskite films with a 10 cm diameter culture dish. As for PEACl-PSCs, 1.0 mg/mL of PEACl dissolved in IPA was spin-coated on perovskite at 5000 rpm for 30 seconds, followed by annealing at 100 ºC for 5 minutes. Then, 20 mg/ml of PCBM dissolved in CB was spin-coated at 1000 rpm for 30 seconds, followed by annealing at 70 ºC for 10 minutes. 0.5 mg/ml of BCP dissolved in IPA was spin-coated at 6000 rpm for 30 seconds, followed by annealing at 70 ºC for 10 minutes. Then, 90 nm thickness of Cu was thermally evaporated as an electrode using a shadow mask. After finishing the device fabrication, 120 nm thickness of MgF_2 anti-reflection coatings were made on the glass side of the textured FTO substrate via thermal evaporation. The evaporation rate is about 1 Å s^{-1}. Finally, the top of the perovskite solar cell was covered with 1.1 mm-thick coverslip glass, which is fixed with a UV-curable resin (ThreeBond Group, 3013B). The solidification of the resin is conducted by UV light illumination for about 30 seconds.

Wide bandgap (WBG) PSCs fabrication

The FTO/NiO_x/Me-4PACz HTL deposition was the same as described above. For deposition of perovskite layer, 1.1 M $Cs_{0.2}FA_{0.8}PbI_{1.9}Br_{1.1}$ precursors were prepared in mixed solvents of DMF and DMSO (4:1 v/v), 5 mol% of excess PbI_2 and 12 mol% MACl were added into the perovskite precursor solution and stirred for 2 hours. 120 μL perovskite solution was dripped on the substrate, followed by a two-step spin-coating of 1000 rpm for 12 seconds and 5000 rpm for 38 seconds. 150 μL CB was

dripped onto the center of film at 12 seconds before the end of spin-coating. The perovskite intermediate phase was subsequently annealed on a hotplate at 100 ºC for 20 minutes. The GMA strategy, PCBM, BCP, Cu and MgF_2 deposition were the same as normal bandgap PSCs.

Narrow bandgap (NBG) PSCs fabrication

The FTO/NiO_x/Me-4PACz HTL deposition was the same as described above. For deposition of perovskite layer, 1.8 M $Cs_{0.1}MA_{0.3}FA_{0.6}Sn_{0.5}Pb_{0.5}I_3$ precursors were prepared in mixed solvents of DMF and DMSO (3:1 v/v), 5 mol% SnF_2 and 2 mol% NH_4SCN were added into the perovskite precursor solution and stirred for 5 hours. 120 μL perovskite solution was dripped on the substrate, followed by a two-step spin-coating of 1000 rpm for 10 seconds and 4000 rpm for 50 seconds. 300 μL CB was dripped onto the center of film at 10 seconds before the end of spin-coating. The perovskite intermediate phase was subsequently annealed on a hotplate at 100 oC for 20 minutes. The GMA strategy, PCBM, BCP, Cu and MgF_2 deposition were the same as normal bandgap PSCs.

Perovskite solar module fabrication

Compared with the fabrication of each functional layer of a small-area solar cell, except for the corresponding increase in the amount of solution, other parameters remain unchanged. A perovskite solar module with 7 series sub-cells was fabricated on a glass/FTO substrate with a size of 6 cm × 6 cm. The series interconnection of modules was realized through P1, P2, and P3 lines. P1, P2, and P3 lines were conducted by a nanosecond laser scribing system (Han's PV-HL0303) and the widths of P1, P2, and P3 are 45, 120, and 60 μm respectively. The distances between P1 and P2 and between P2 and P3 were ca. 40 μm.

DFT calculation

We used the DFT as implemented in the Vienna Ab initio simulation package (VASP) in all calculations. The exchange-correlation potential is described by using the

generalized gradient approximation of Perdew-Burke-Ernzerhof (GGA-PBE). The projector augmented-wave (PAW) method is employed to treat interactions between ion cores and valence electrons. The plane-wave cutoff energy was fixed to 400 eV. A Monkhorst-Pack k-mesh with a 2 × 2 × 1 k-point grid was used for structural optimization. The structural models were relaxed until the Hellmann-Feynman forces smaller than -0.02 eV/Å and the change in energy smaller than 10-5 eV was attained. The long-range van der Waals interaction is described by the DFT-D3 approach. The adsorption energy (*E*ads) of species is calculated by:

$$E\text{ads} = E(\text{system}) - E(\text{catalyst}) - E(\text{species})$$

where *E*(system), *E*(catalyst), and *E*(species) are the total energy of the optimized system with adsorbed species, the isolated catalyst, and species, respectively.

Ab initio molecular dynamics (AIMD)

CP2K was employed to carry out the theoretical calculations in the framework of DFT. CP2K/Quickstep employed two representations of the electron density: localized Gaussian and plane wave basis sets. For the Gaussian-based (localized) expansion of the Kohn-Sham orbitals, we used a library of contracted molecularly optimized valence double-zeta plus polarization basis sets, and the complementary plane wave basis set had a cutoff of 400 Rydberg for the electron density. The generalized gradient corrected approximation of Perdew, Burke and Ernzerhof (PBE) was adopted to relax the geometric structures. The dispersion correction was applied in all calculations with the GrimmeD3 method. For sampling the structures of intermediate phase, the canonical ensemble (NVT) conditions were imposed by a Nose-Hoover thermostat with the temperature of 370 K.

Characterizations

Gas chromatography-mass spectrometry (GC-MS) was measured by 7890A-5975C (Agilent Technologies, USA). Scanning electron microscope (SEM) images was measured by JSM-7800F (JEOL, China). Atomic force microscope (AFM) was measured by MFP-3D (Oxford, UK). X-ray photoelectron spectroscopy (XPS) and ultraviolet photoelectron spectroscopy (UPS) were measured by AXIS Ultra DLD (China) with an Al Kα X-ray source and He Iα photon source (21.2 eV) respectively. X-ray diffraction (XRD) pattern was measured by Mini Flex 600 (Rigaku, Japan) using Cu Kα radiation. Raman atlas and photoluminescence (PL) mapping was measured by inVia Qontor (Renishaw, UK). PL and time-resolved PL (TRPL) were measured by FLS1000 (Edinburgh Instruments, UK). UV-vis absorption spectra were measured by Shimadzu UV 2450 spectrometry. The time-of-flight secondary ion mass spectroscopy (TOF-SIMS) was performed with an IONTOF TOF.SIMS 5-100 instrument. Ar cluster (10 keV) was used in the sputtering and Bi^{3+} (30 keV) was used to probe the sample with an analysis area of 100 × 100 μm^2.

Current density-voltage (*J-V*) curves of PSCs were measured by a Keithley 2400 digital source meter under a simulated solar source of AM1.5 G (100 mW cm^{-2}, Wacom Denso Co., Japan). The measurement was conducted forward (from -0.2 to 1.3 V) scan or reverse (from 1.3 to -0.2 V) scan. The delay time and step voltage were set as 20 ms and 20 mV, respectively. The external quantum efficiency (EQE) spectra were performed with director current mode (CEP-2000BX, Bunko-Keiki).

The electrochemical impedance spectroscopy (EIS), dark current, Mott-Schottky analysis, thermal admittance spectroscopy (TAS) and drive-level capacitance profiling (DLCP) were performed on Zahner, Germany. For the Mott-Schottky analysis, the DC bias was scanning from 0.5 V to the 1.3 V. The amplitude of the AC bias was 20 mV. The DLCP measurement were conducted in the same DC bias range with that for the standard *C-V* measurement at 100 kHz.[43,44] While the amplitude of the AC biases was ranging from 20 to 200 mV. For the TAS measurement, the DC bias was fixed at 0 V

and the amplitude of the AC bias was 20 mV. The scanning range of the AC frequency was 1 - 100 kHz. The transient photovoltage (TPV) and transient photocurrent (TPC) test were performed on an attenuated UV laser pulse (SRS NL 100 Nitrogen Laser) under 1-sun illumination. The laser wavelength is 337 nm, the repeating frequency was about 20 Hz, and the pulse width was less than 3.5 ns.

For storage stability (following the testing procedures of the ISOS-D-1 protocols), the devices were put into drying oven with the temperature of 25 ºC, humidity of RH 20% under dark. For heat stability (following the testing procedures of the ISOS-D-2 protocols), the devices were put into environment chamber with the temperature of 85 ºC, humidity of RH 35% under dark. For operational stability (following the testing procedures of the ISOS-L-1 protocols), the MPP tracking was performed with a solar cell light resistance testing system (Bunkoukeiki, Japan) under a white LED light with 1 sun equivalent intensity and continuous bias voltage, and the temperature was around 45 ºC. The J-V curves under forward scans were recorded every 10 hours during the whole test. The maximum power points were obtained from the J-V curves and were also adjusted every 10 hours.

Supplementary Figures and Tables

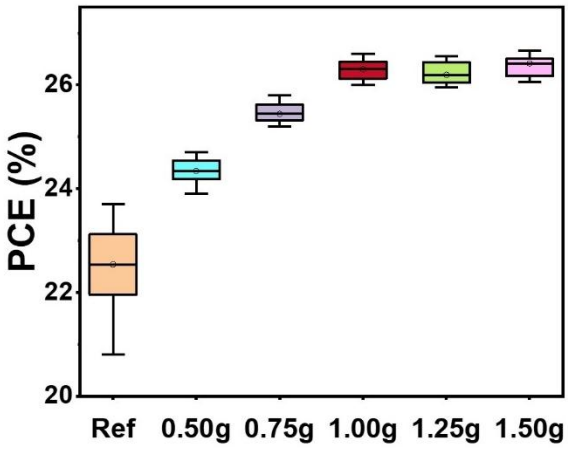

Figure S1. The relationship between the statistics of PCEs distribution and the dosage of ammonium dithiocarbamate powder. Twenty devices were fabricated for each batch.

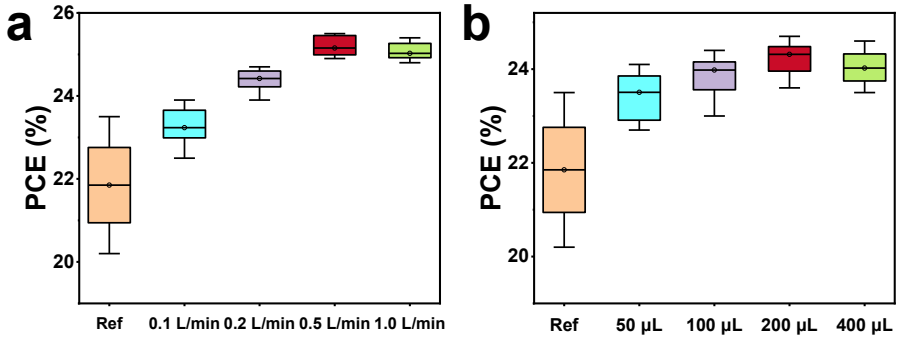

Figure S2. The relationship between the statistics of PCEs distribution and the dosage of (a) NH_3 and (b) CS_2. Twenty devices were fabricated for each batch.

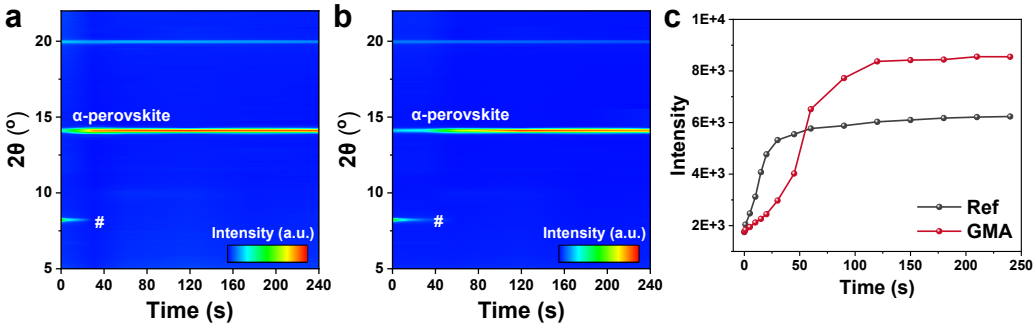

Figure S3. In-situ XRD of (a) Ref- and (b) GMA-perovskite films. # denotes the peaks of intermediate phase. (c) XRD intensity evolution of the featured peak at 14.1°.

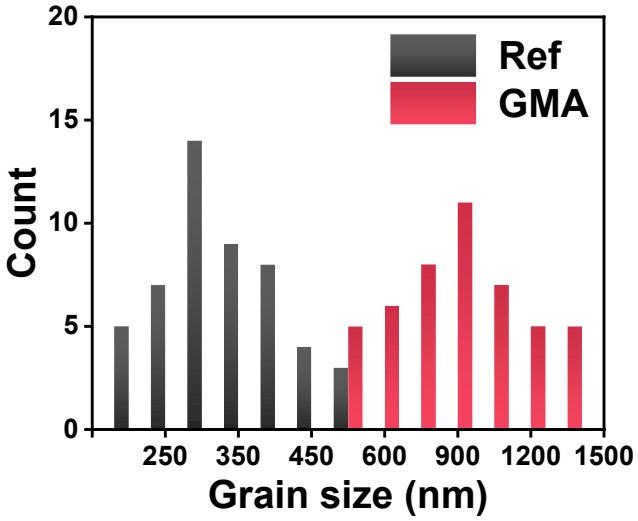

Figure S4. Grain size distribution of the Ref- and GMA-perovskite films.

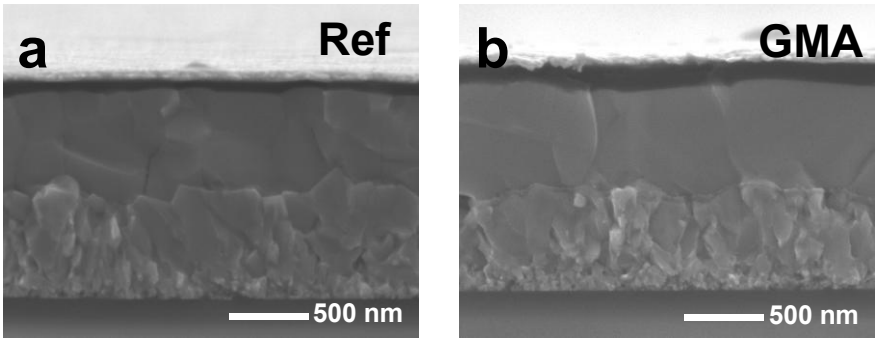

Figure S5. Cross-section SEM images of (a) Ref- and (b) GMA-devices.

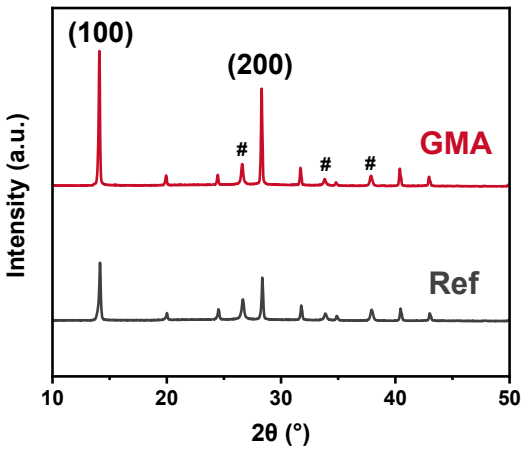

Figure S6. XRD patterns of Ref- and GMA-perovskite films, in which # represents the diffraction peak of FTO.

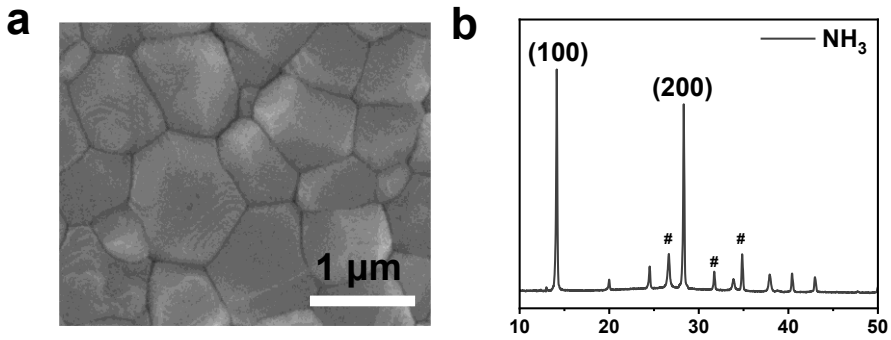

Figure S7. (a) SEM and (b) XRD of the perovskite film annealed in NH_3.

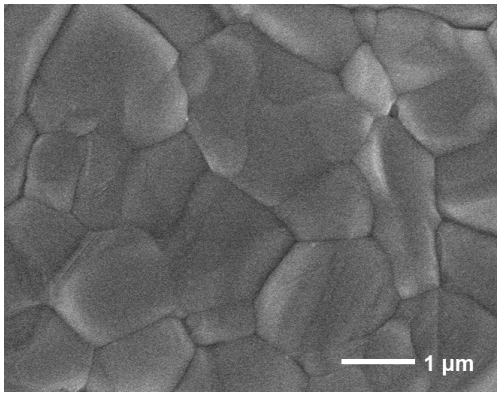

Figure S8. Top-view SEM image of the perovskite film annealed in air (RH 35%) at 150 ºC for 20 minutes. 150 ºC is usually required for H_2O-perovskite to realize the phase transformation from δ to α.[2,3]

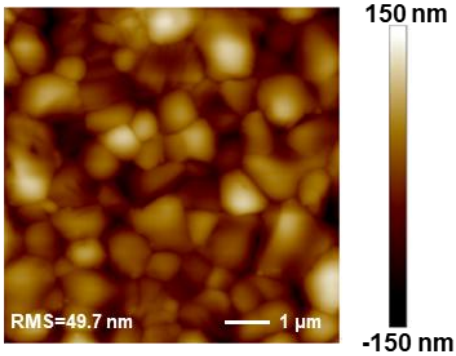

Figure S9. AFM image of the perovskite film annealed in air (RH 35%) at 150 ºC for 20 minutes.

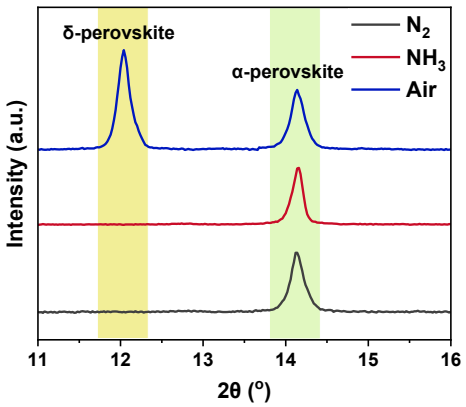

Figure S10. XRD patterns of the perovskite intermediate phases exposed to different atmosphere for 10 minutes. RH 35% is controlled for air-sample.

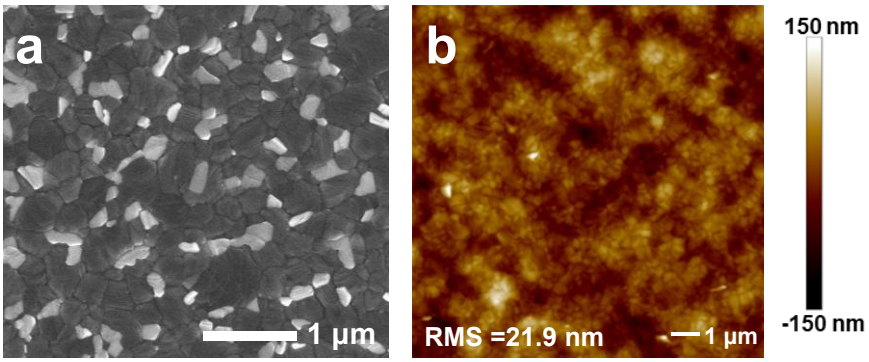

Figure S11. (a) SEM and (b) AFM images of the perovskite film annealed in CS_2.

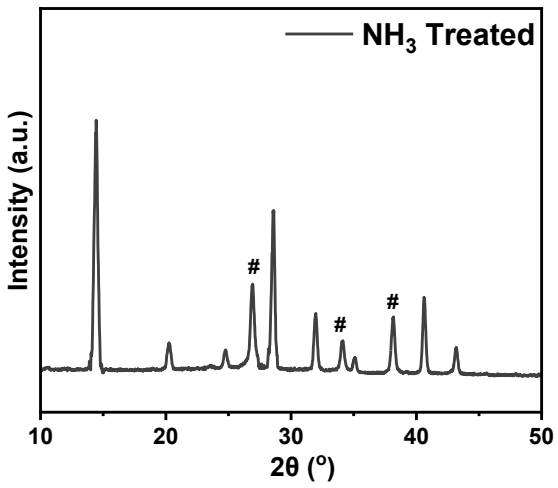

Figure S12. XRD pattern of Ref-perovskite post-treated with NH_3 for 20 minutes, in which # represents the diffraction peak of FTO. The ratio between the characteristic peaks of perovskite and FTO is unchanged, compared with that of Ref-perovskite XRD pattern in Fig. S6.

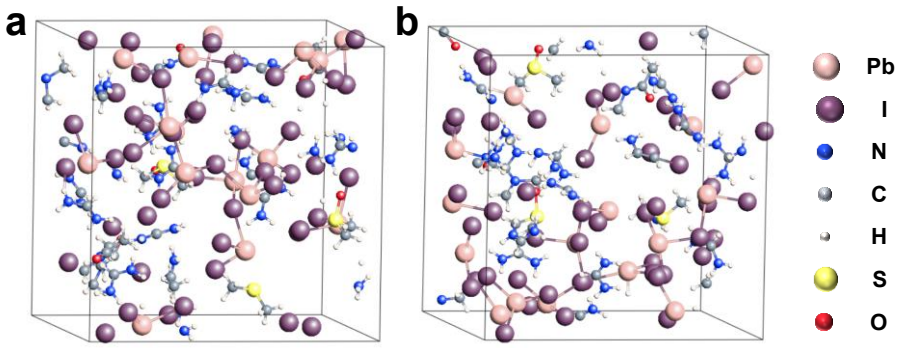

Figure S13. Ab initio MD simulations of perovskites precursors (a) without or (b) with NH_3.

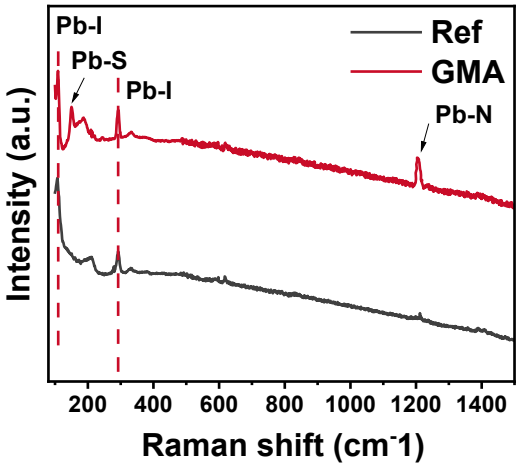

Figure S14. Raman spectra of the Ref- and GMA-perovskite films.

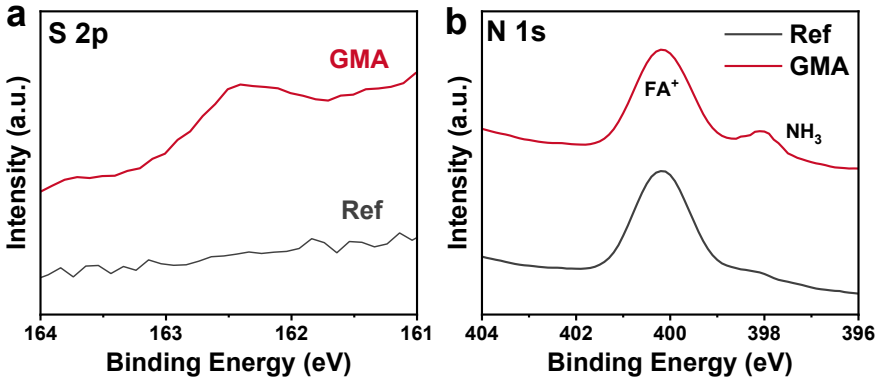

Figure S15. XPS spectra of (a) S 2p and (b) N 1s for the Ref- and GMA- perovskite films.

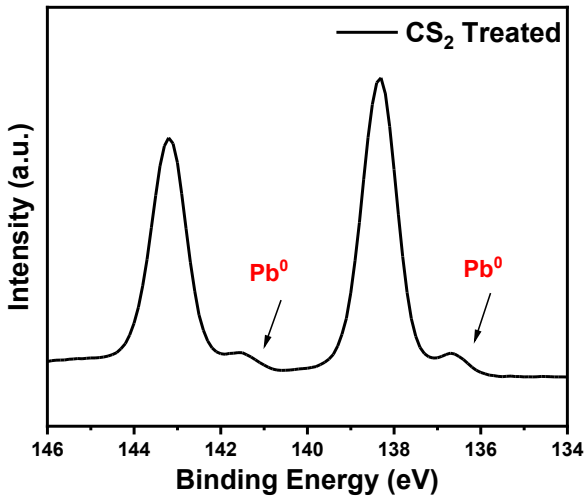

Figure S16. XPS spectra of Pb 4f for the CS_2 post-treated perovskite film. The obtained Ref-perovskite was annealed in CS_2 gas atmosphere for 20 minutes.

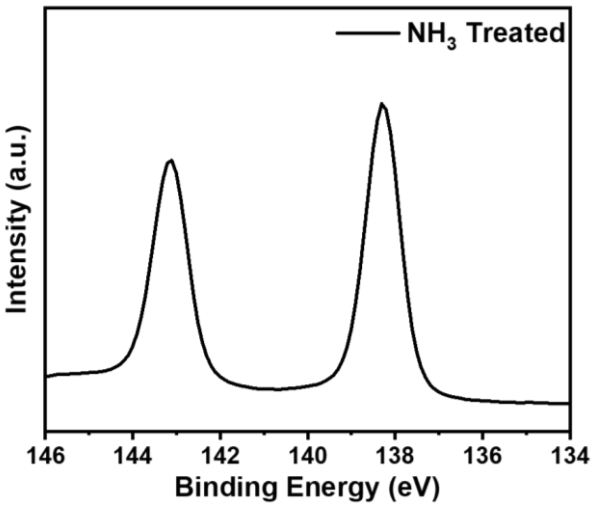

Figure S17. XPS spectra of Pb 4f for the NH_3 post-treated perovskite film. The obtained Ref-perovskite was annealed in NH_3 gas atmosphere for 20 minutes.

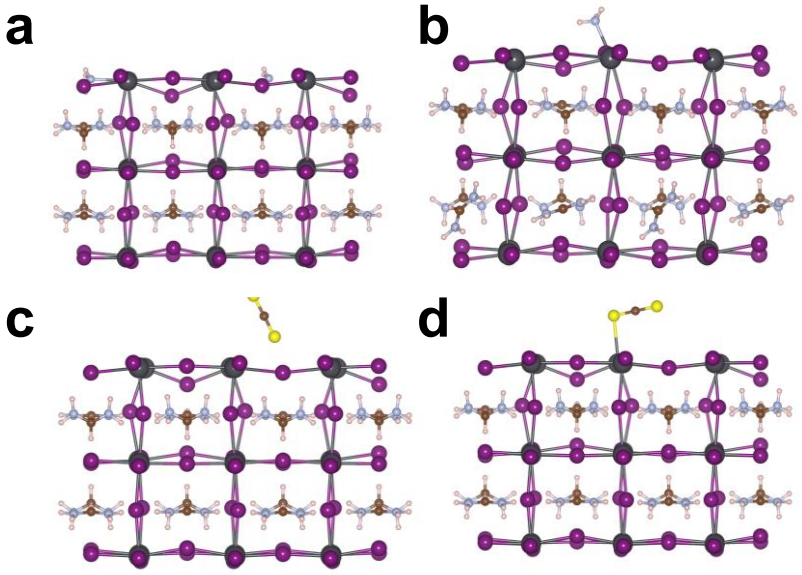

Figure S18. NH_3 (a) adsorbs on I^- vacancies and (b) coordinates with the undercoordinated Pb^{2+} of perovskite based on DFT calculations. CS_2 (c) adsorbs on I^- vacancies and (d) coordinates with the undercoordinated Pb^{2+} of perovskite based on DFT calculations.

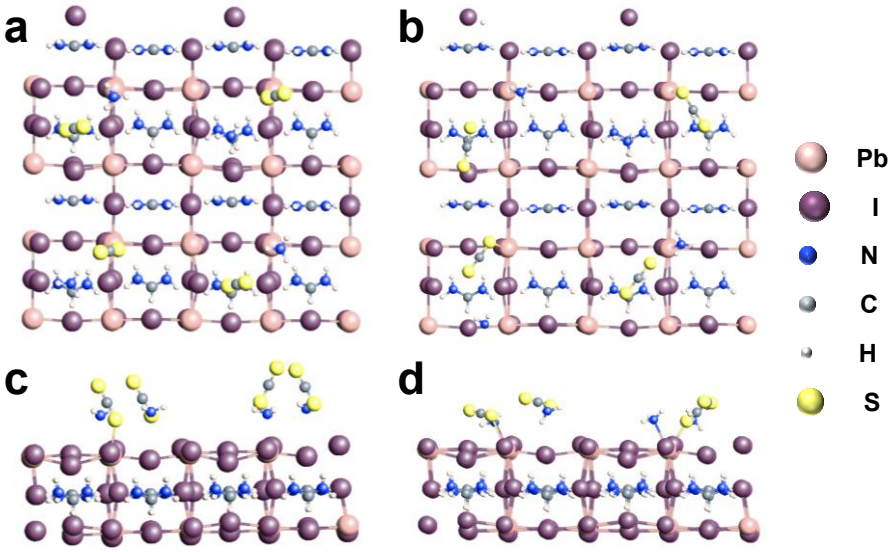

Figure S19. Top view of (a) initial state and (b) final state of the NH_3 and CS_2 co-adsorption based on MD simulations. Cross-sectional view of (c) initial state and (d) final state of the NH_3 and CS_2 co-adsorption based on MD simulations.

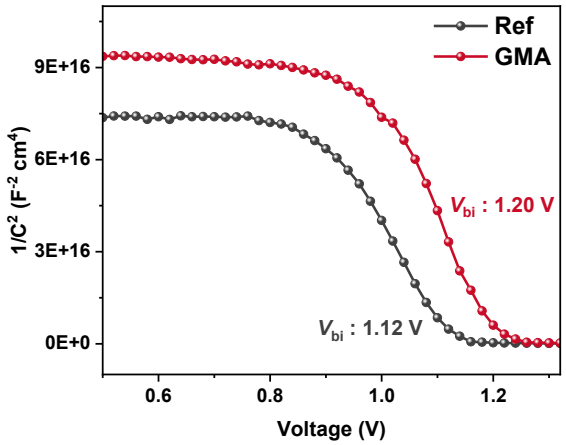

Figure S20. Mott-Schottky plots of the Ref- and GMA-devices, obtained under dark conditions.

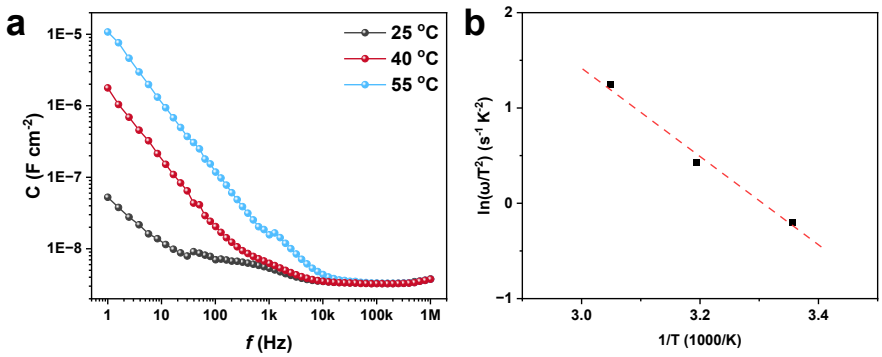

Figure S21. (a) C-*f* curves measured under different temperature. (b) Arrhenius plot of the characteristic frequencies under different temperature.

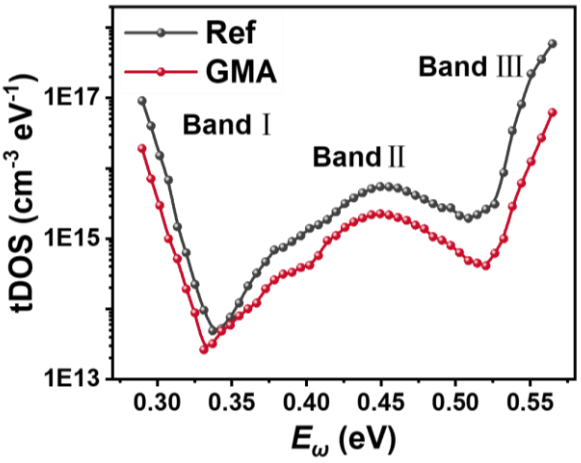

Figure S22. tDOS of Ref- and GMA-devices, exhibiting three distinct trap bands.

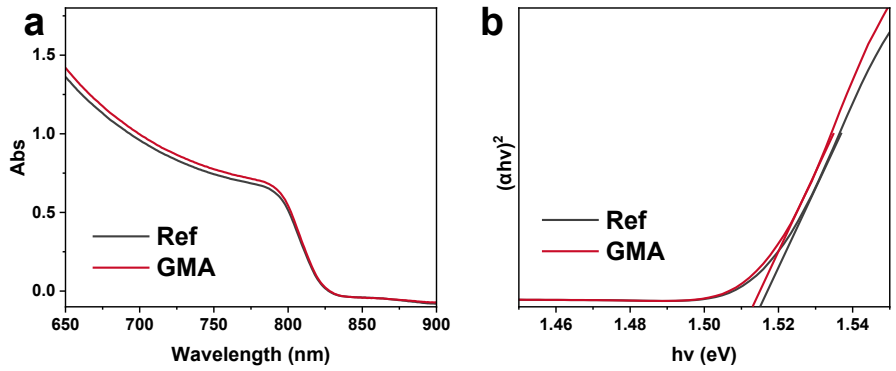

Figure S23. (a) UV-vis spectra and (b) Tauc curves of the Ref- and GMA- perovskite films.

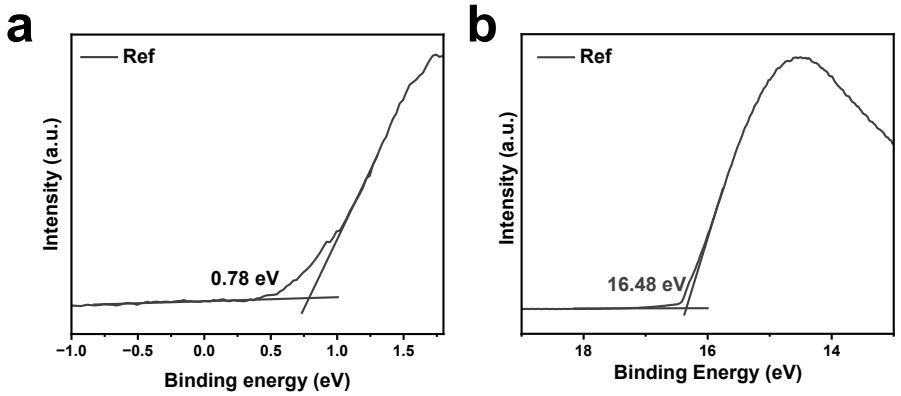

Figure S24. UPS spectra for Ref-perovskite film.

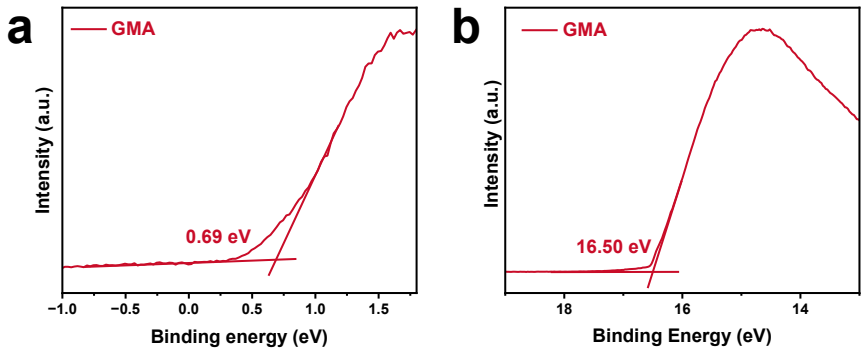

Figure S25. UPS spectra for GMA-perovskite film.

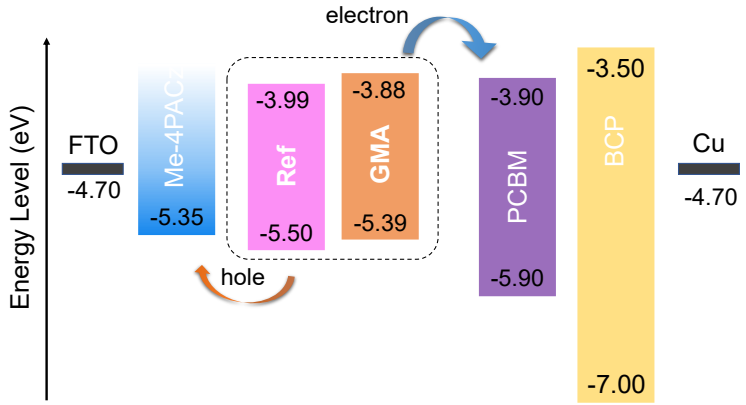

Figure S26. Energy level diagram of the Ref- and GMA-devices. The energy levels of Ref-and GMA-perovskite is derived from Fig. S24, S26. The energy levels of the other layers are obtained from the literature.[5,6]

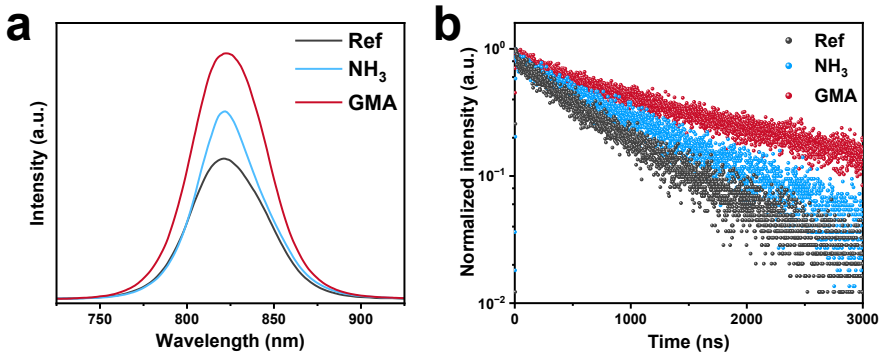

Figure S27. (a) Steady-state PL spectra and (b) TRPL spectra of Ref-, NH_3- and GMA-perovskite films, respectively.

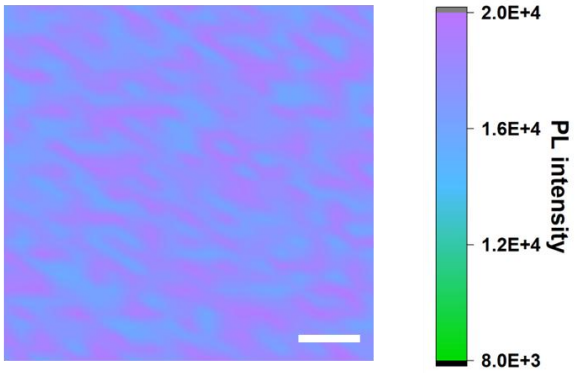

Figure S28. Mapping of the PL intensity for PEACl-perovskite film. The scale bar is 5 μm.

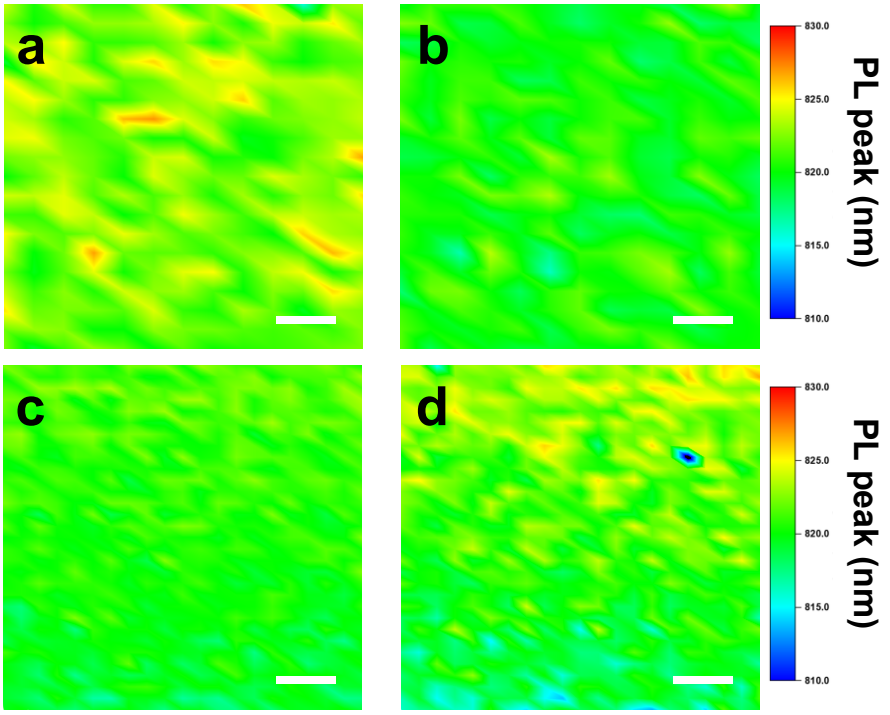

Figure S29. Mapping of the PL peak position for (a) Ref-, (b) NH_3-, (c) GMA- and (d) PEACl-perovskite films. The scale bar is 5 μm.

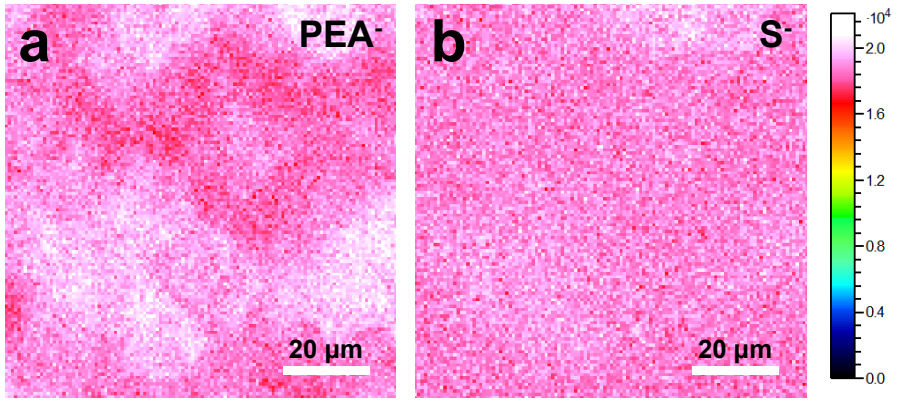

Figure S30. Two-dimensional imaging of passivator distribution obtained by TOF-SIMS for perovskite films based on (a) traditional solution-based passivation and (b) GMA method.

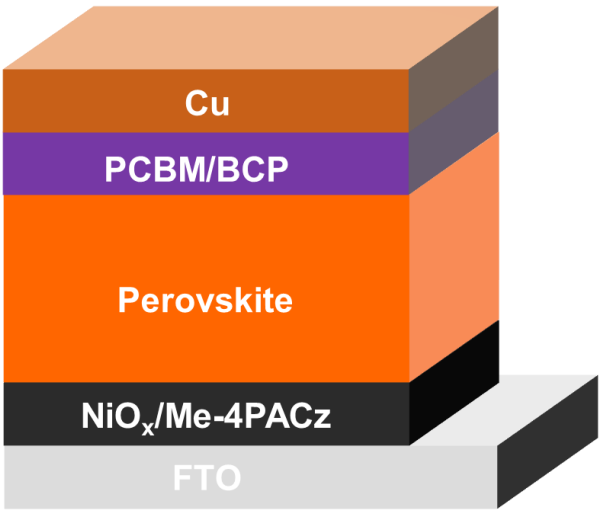

Figure S31. Structure diagram of the device.

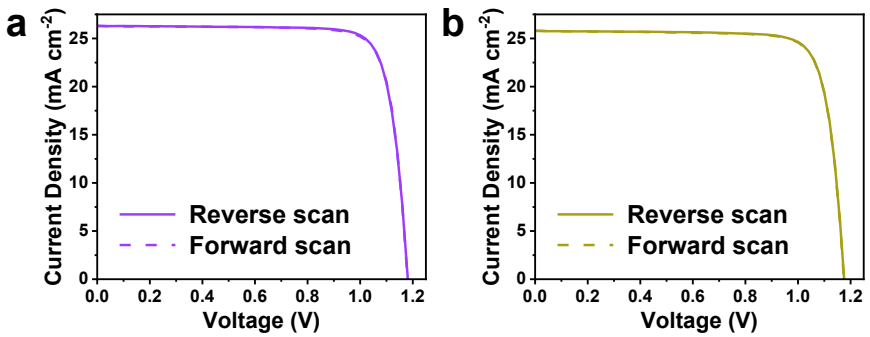

Figure S32. *J-V* curves of (a) NH_3- and (b) CS_2 devices with an aperture area of 0.06 cm^2.

Test and Calibration Center of New Energy Device and Module,
Shanghai Institute of Microsystem and Information Technology,
Chinese Academy of Sciences (SIMIT)

Measurement Report

Report No. 24TR092805

Client Name	Shanghai Jiao Tong University
Client Address	800 Dongchuan Road, Minhang District, Shanghai
Sample	Perovskite solar cell
Manufacturer	Shanghai Jiao Tong University
Measurement Date	28th September, 2024

Performed by:	Qiang Shi	**Date:** 28/09/2024
Reviewed by:	Wenjie Zhao	**Date:** 28/09/2024
Approved by:	Yucheng Liu	**Date:** 28/09/2024

Address: No.235 Chengbei Road, Jiading, Shanghai **Post Code:**201800
E-mail: solarcell@mail.sim.ac.cn **Tel:** +86-021-69976905

Sample Information

Sample Type	Perovskite solar cell
Serial No.	13-12-3
Lab Internal No.	24092801-5#
Measurement Item	I-V characteristic
Measurement Environment	24.8±2.0°C, 40.3±5.0%R.H

Measurement of I-V characteristic

Reference cell	PVM1121
Reference cell Type	mono-Si, WPVS, calibrated by NREL (Certificate No. ISO 2098)
Calibration Value/Date of Calibration for Reference cell	143.95mA/ Feb. 2024
Measurement Conditions	Standard Test Condition (STC): Spectral Distribution: AM1.5, Irradiance: 1000±50W/m², Temperature: 25±2°C
Measurement Equipment/ Date of Calibration	AAA Steady State Solar Simulator (YSS-T155-2M) / Sep.2023 IV test system (ADCMT 6246) / June. 2024 Measuring Microscope (MF-B2017C) / July.2024
Measurement Method	I-V Measurement: Dual-lamp solar simulator spectral distribution adjusted to make the match factor within 1.00±0.01, Irradiance adjusted to 1 Sun according to reference cell calibration value. Logarithmic sweep in both directions (Voc to Isc and Isc to Voc) during one flash based on IEC 60904-1:2020
Measurement Uncertainty	Area: 1.0%(k=2); Isc: 2.1%(k=2); Voc: 1.0%(k=2); Pmax: 2.5%(k=2); Eff: 2.6%(k=2)

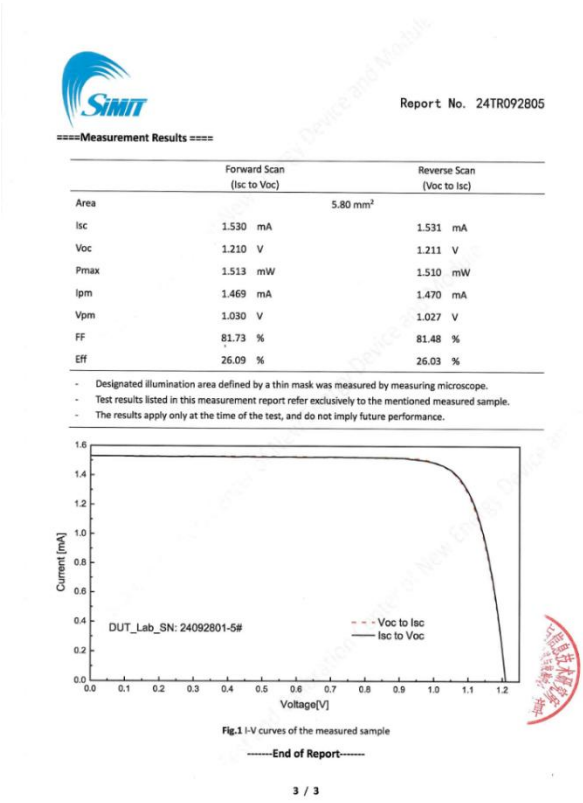

Report No. 24TR092805

====Measurement Results ====

	Forward Scan (Isc to Voc)	Reverse Scan (Voc to Isc)
Area	5.80 mm²	
Isc	1.530 mA	1.531 mA
Voc	1.210 V	1.211 V
Pmax	1.513 mW	1.510 mW
Ipm	1.469 mA	1.470 mA
Vpm	1.030 V	1.027 V
FF	81.73 %	81.48 %
Eff	26.09 %	26.03 %

- Designated illumination area defined by a thin mask was measured by measuring microscope.
- Test results listed in this measurement report refer exclusively to the mentioned measured sample.
- The results apply only at the time of the test, and do not imply future performance.

Fig.1 I-V curves of the measured sample

-------End of Report-------

3 / 3

Figure S33. Certification report of GMA-device. Tested by Shanghai Institute of Microsystem and Information Technology (SIMIT), Chinese Academy of Sciences (CAS).

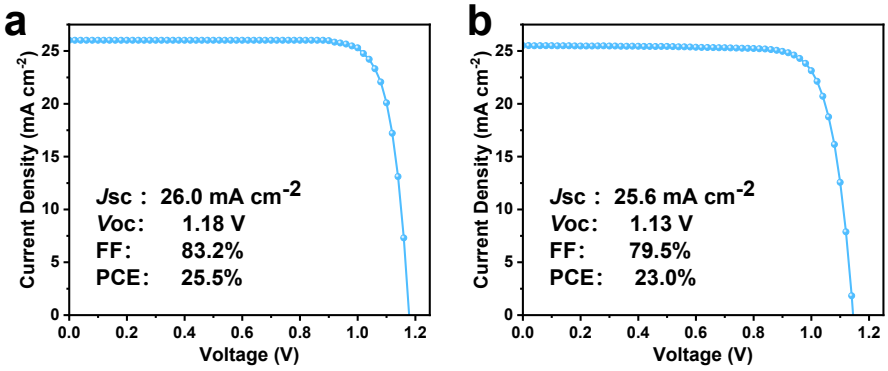

Figure S34. *J-V* curves of PEACl-devices with an aperture area of (a) 0.06 cm^2 and (b) 1.02 cm^2.

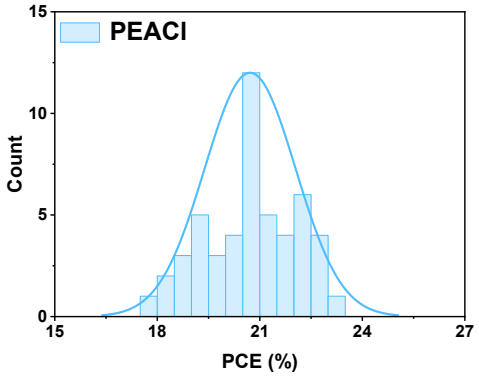

Figure S35. The efficiency statistics of fifty PEACl-devices with an aperture area of 1.02 cm^2.

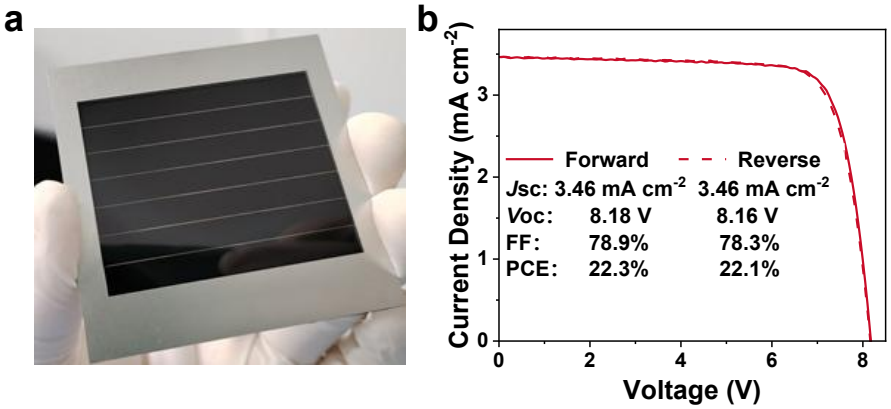

Figure S36. (a) Optical photos and (b) *J-V* curves of the GMA-PSMs with an aperture area of 20.3 cm^2.

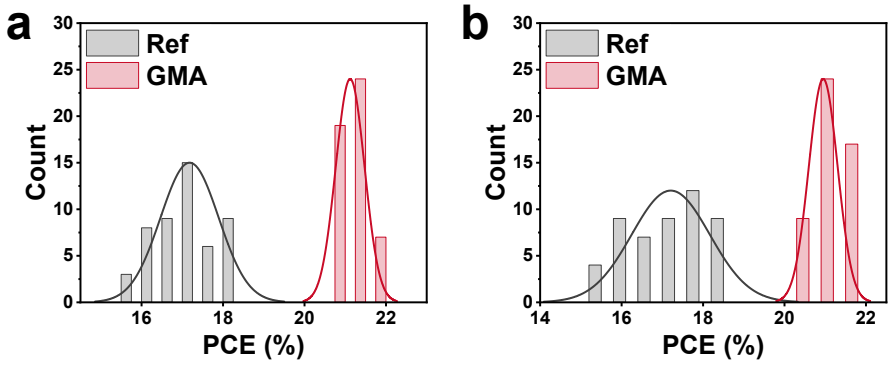

Figure S37. The statistics of PCEs for fifty Ref- and GMA- devices with (a) wide bandgap and (b) narrow bandgap perovskite (aperture area, 1.02 cm^2).

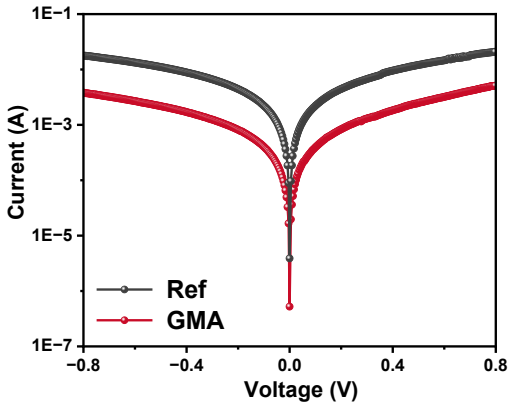

Figure S38. Dark current of the Ref- and GMA-devices.

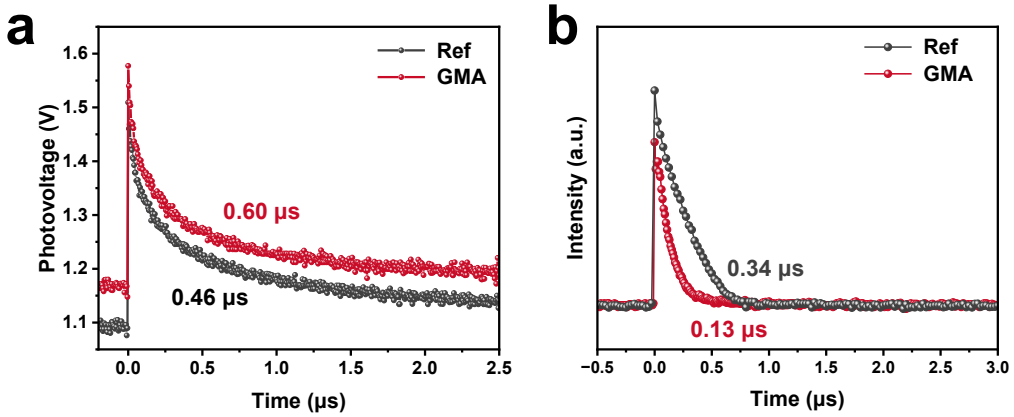

Figure S39. (a) TPV and (b) TPC curves of the Ref- and GMA-devices.

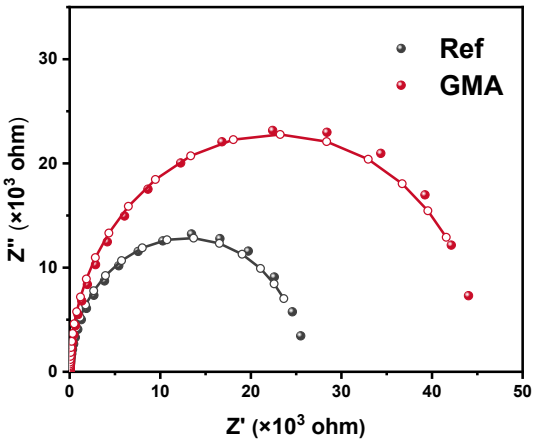

Figure S40. Nyquist plots of the Ref- and GMA-devices recorded at 0.8 V in dark condition.

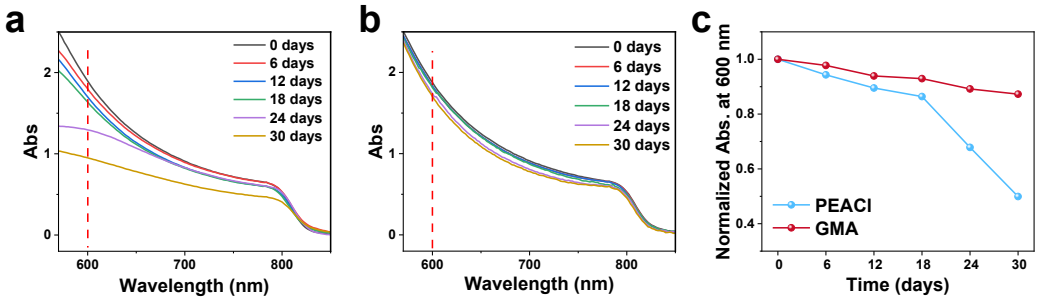

Figure S41. UV-vis spectra of (a) PEACl- and (b) GMA-perovskite films during 30 days of ageing test under 1-sun illumination. (c) Normalized absorbance evolution at 600 nm in the UV-vis spectra of PEACl- and GMA-perovskite films. The perovskite films were not encapsulated (exposure condition: 25 ºC and RH 35%).

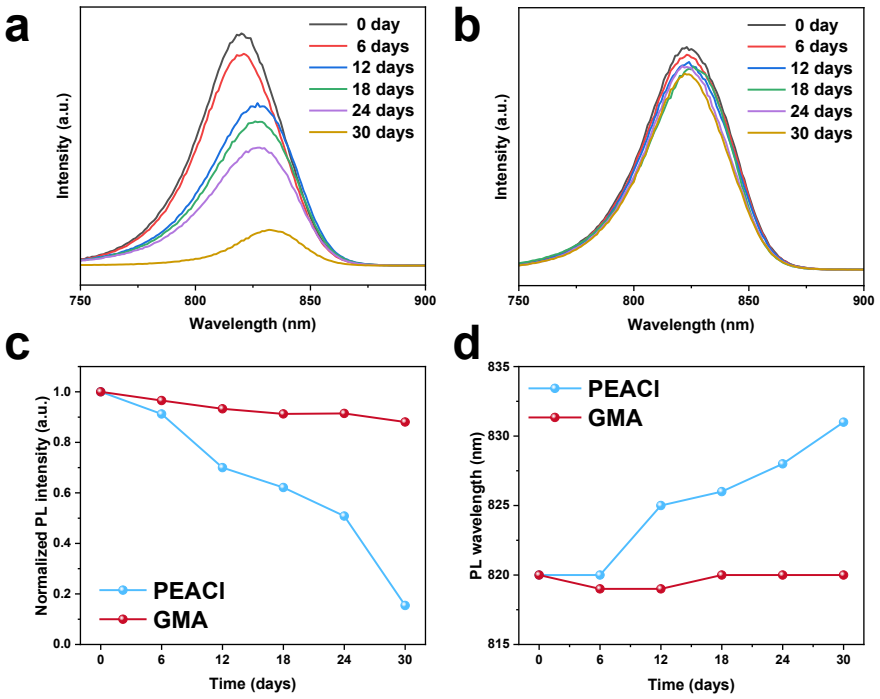

Figure S42. Steady-state PL spectra of the (a) PEACl- and (b) GMA-perovskite films during 30 days of ageing test under 1-sun illumination. (c) Normalized PL intensity and (d) PL peak position evolution of the PEACl- and GMA-perovskite films. The perovskite films were not encapsulated (exposure condition: 25 °C and RH 35%).

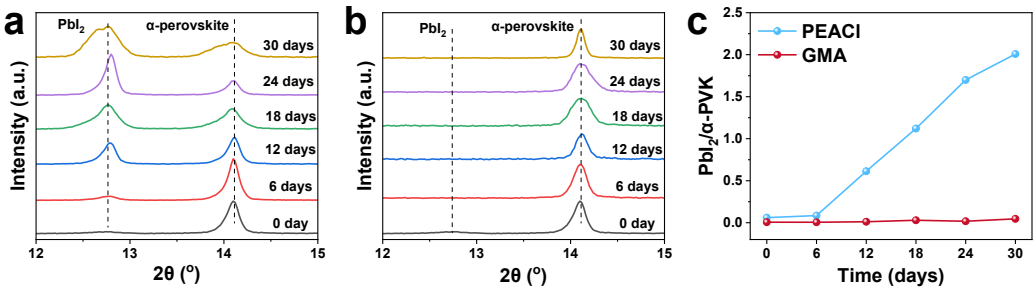

Figure S43. XRD patterns of the (a) PEACl- and (b) GMA-perovskite films during 30 days of ageing test under 1-sun illumination. (c) The ratio evolution of the characteristic XRD peaks of PbI_2 and perovskite. The perovskite films were not encapsulated (exposure condition: 25 °C and RH 35%).

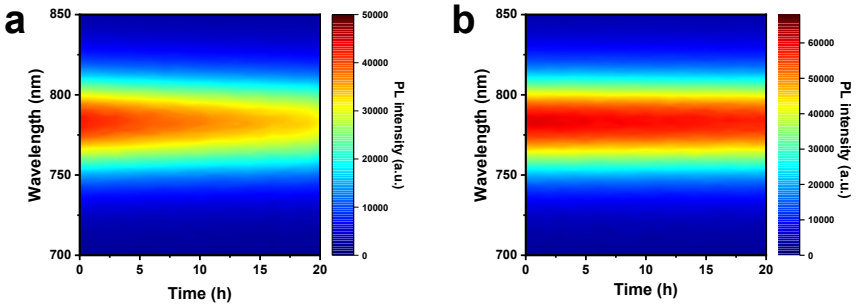

Figure S44. In situ PL intensity of the (a) PEACl- and (b) GMA-perovskite films ageing under 85 °C and RH 85% for 20 hours. The perovskite films were not encapsulated.

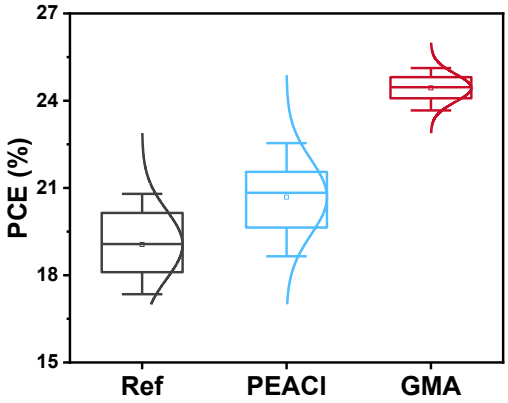

Figure S45. The initial PCEs of the Ref-, PEACl- and GMA-devices for the ISOS-D-1 stability test. Ten devices were tested for each batch.

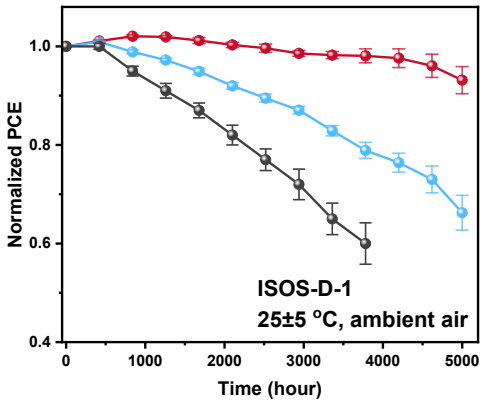

Figure S46. ISOS-D-1 stability test of the Ref-, PEACl- and GMA-devices. Ten devices were tested for each batch.

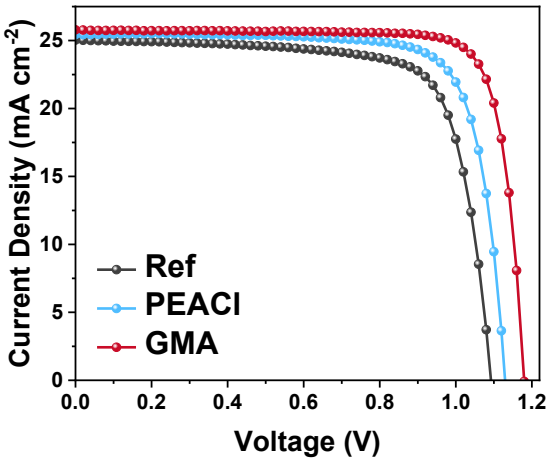

Figure S47. The initial *J-V* curves of Ref-, PEACl- and GMA-devices for the ISOS-D-2 stability test.

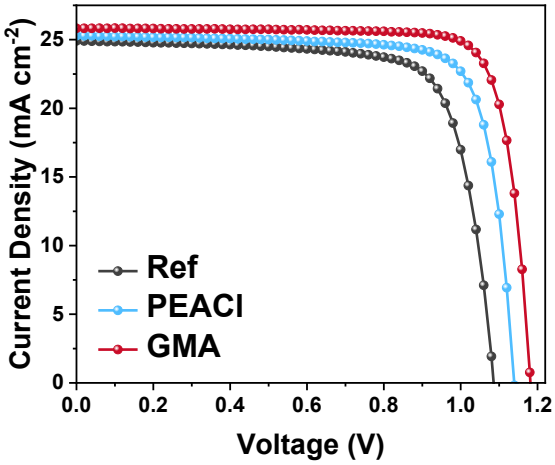

Figure S48. The initial *J-V* curves of Ref-, PEACl- and GMA-devices for the ISOS-L-1 stability test.

Table S1. PLQY and QFLS of the Ref-, NH_3- and GMA-perovskite films.

	PLQY (%)	***E*g (eV)**	**QFLS (eV)**
Ref	0.82	1.51	1.14
NH_3	3.88	1.51	1.18
GMA	18.42	1.51	1.22

Table S2. Photovoltaic parameters of the champion Ref-, NH_3-, CS_2- and GMA-devices.

		V_{OC} (V)	J_{SC} (mA cm^{-2})	FF (%)	PCE (%)
Ref	Forward	1.13	25.9	80.1	23.5
	Reverse	1.14	25.8	80.8	23.7
NH_3	Forward	1.18	26.3	81.8	25.4
	Reverse	1.18	26.3	82.2	25.5
CS_2	Forward	1.18	25.8	81.1	24.7
	Reverse	1.18	25.8	81.1	24.7
GMA	Forward	1.22	26.4	82.5	26.6
	Reverse	1.22	26.4	82.6	26.6

Table S3. Energy loss of PSCs in recent works.

Perovskite composition	*Eg* (eV)	V_{OC} (V)	Energy loss (V)	Ref
$Cs_{0.05}FA_{0.95}PbI_3$	**1.51**	**1.22**	**0.29**	**Our work**
$Cs_{0.1}FA_{0.9}PbI_3$	1.55	1.18	0.37	6
$(FA_{0.98}MA_{0.02})_{0.95}Cs_{0.05}PbI_{2.94}Br_{0.06}$	1.55	1.18	0.37	7
$Cs_{0.05}MA_{0.05}FA_{0.90}PbI_3$	1.53	1.17	0.36	8
$FAPbI_3$	1.54	1.16	0.38	9
$Cs_{0.05}FA_{0.85}MA_{0.1}PbI_3$	1.53	1.18	0.35	10
$Cs_{0.05}(FA_{0.95}MA_{0.05})_{0.95}PbI_{2.85}Br_{0.15}$	1.55	1.17	0.36	11
$Cs_{0.1}FA_{0.9}PbI_3$	1.55	1.17	0.38	12
$FAPbI_3$	1.54	1.17	0.37	13
$FA_{0.95}Cs_{0.05}PbI_3$	1.51	1.16	0.35	14
$Cs_{0.05}(FA_{0.98}MA_{0.02})_{0.95}PbI_3$	1.55	1.18	0.37	15
$FAPbI_3$	1.54	1.17	0.37	16
$FA_{0.85}MA_{0.15}Pb(I_{0.85}Br_{0.15})_3$	1.61	1.26	0.35	17
$FA_{0.8}Cs_{0.2}PbI_{1.8}Br_{1.2}$	1.77	1.34	0.43	18
$Cs_{0.1}FA_{0.9}PbI_3$	1.55	1.18	0.37	19
$FA_{0.95}Cs_{0.05}PbI_3$	1.55	1.20	0.35	20
$FAPbI_3$	1.54	1.19	0.35	21
$Rb_{0.05}Cs_{0.05}MA_{0.05}FA_{0.85}Pb(I_{0.95}Br_{0.05})_3$	1.54	1.16	0.38	22
$FA_{0.95}Cs_{0.05}PbI_3$	1.51	1.16	0.35	23
$Cs_{0.05}MA_{0.1}FA_{0.85}PbI_3$	1.54	1.16	0.38	24
$FAPbI_3$	1.54	1.19	0.35	25

Table S4. Certified V_{OC} of high-performance PSCs (certified PCE > 26%).

Perovskite composition	Certified V_{OC} (V)	Year	Ref
$Cs_{0.05}FA_{0.95}PbI_3$	**1.21**	**2025**	**Our work**
$Cs_{0.1}FA_{0.9}PbI_3$	1.17	2024	6
$FAPbI_3$	1.17	2024	16
$Cs_{0.05}FA_{0.95}PbI_3$	1.19	2024	20
$FAPbI_3$	1.19	2024	21
$Cs_{0.1}FA_{0.9}PbI_3$	1.17	2024	26
$FAPbI_3$	1.17	2024	27
$Cs_{0.05}(FA_{0.95}MA_{0.05})_{0.95}PbI_{2.85}Br_{0.15}$	1.19	2024	27
$FA_{0.92}MA_{0.08}PbI_3$	1.19	2024	29
$Cs_{0.05}(FA_{0.98}MA_{0.02})_{0.95}Pb(I_{0.98}Br_{0.02})_3$	1.18	2025	30
$Cs_{0.05}(FA_{0.98}MA_{0.02})_{0.95}Pb(I_{0.98}Br_{0.02})_3$	1.20	2025	31

Table S5. Photovoltaic parameters of the champion Ref- and GMA- devices with an aperture area of 1.02 cm^2.

		V_{OC} (V)	**J_{SC} (mA cm^{-2})**	**FF (%)**	**PCE (%)**
Ref	Forward	1.11	25.0	74.6	20.7
	Reverse	1.10	25.0	75.6	20.8
GMA	Forward	1.18	25.9	82.0	25.1
	Reverse	1.18	26.0	81.8	25.1

Table S6. Electrochemical parameters of the Ref- and GMA-PSCs.

	Rs (Ω)	**Rrec (×10^3 Ω)**	**Crec (×10^{-9} F)**	***ε***
Ref	34.64	25.70	5.746	43.26
GMA	31.42	45.55	5.361	40.36

References

1. F. Ye, H. Chen, F. Xie, W. Tang, M. Yin, J. He, E. Bi, Y. Wang, X. Yang and L. Han, *Energy Environ. Sci.* 2016, **9**, 2295-2301.
2. J. Park, J. Kim, H.-S. Yun, M. J. Paik, E. Noh, H. J. Mun, M. G. Kim, T. J. Shin and S. I. Seok, *Nature*, 2023, **616**, 724-730.
3. Z. Shen, Q. Han, X. Luo, Y. Shen, Y. Wang, Y. Yuan, Y. Zhang, Y. Yang and L. Han, *Nat. Photonics* 2024, **18**, 450-457.
4. A. Al-Ashouri, E. Köhnen, B. Li, A. Magomedov, H. Hempel, P. Caprioglio, J. A. Márquez, A. B. Morales Vilches, E. Kasparavicius, J. A. Smith, N. Phung, D. Menzel, M. Grischek, L. Kegelmann, D. Skroblin, C. Gollwitzer, T. Malinauskas, M. Jošt, G. Matič, B. Rech, R. Schlatmann, M. Topič, L. Korte, A. Abate, B. Stannowski, D. Neher, M. Stolterfoht, T. Unold, V. Getautis and S. Albrecht, *Science* 2020, **370**, 1300-1309.
5. Y. Chen, Z. Yang, S. Wang, X. Zheng, Y. Wu, N. Yuan, W.-H. Zhang and S. Liu, *Adv. Mater.* 2018, **30**, 1805660.
6. H. Chen, C. Liu, J. Xu, A. Maxwell, W. Zhou, Y. Yang, Q. Zhou, A. S. R. Bati, H. Wan, Z. Wang, L. Zeng, J. Wang, P. Serles, Y. Liu, S. Teale, Y. Liu, M. I. Saidaminov, M. Li, N. Rolston, S. Hoogland, T. Filleter, M. G. Kanatzidis, B. Chen, Z. Ning and E. H. Sargent, *Science* 2024, **384**, 189-193.
7. K. Zhao, Q. Liu, L. Yao, C. Değer, J. Shen, X. Zhang, P. Shi, Y. Tian, Y. Luo, J. Xu, J. Zhou, D. Jin, S. Wang, W. Fan, S. Zhang, S. Chu, X. Wang, L. Tian, R. Liu, L. Zhang, I. Yavuz, H.-f. Wang, D. Yang, R. Wang, J. Xue, *Nature* 2024, **632**, 301-306.
8. C. Liu, Y. Yang, H. Chen, J. Xu, A. Liu, A. S. R. Bati, H. Zhu, L. Grater, S. S. Hadke, C. Huang, V. K. Sangwan, T. Cai, D. Shin, L. X. Chen, M. C. Hersam, C. A. Mirkin, B. Chen, M. G. Kanatzidis and E. H. Sargent, *Science* 2023, **382**, 810-815.
9. S. Yu, Z. Xiong, H. Zhou, Q. Zhang, Z. Wang, F. Ma, Z. Qu, Y. Zhao, X. Chu, X. Zhang and J. You. *Science* 2023, **382**, 1399-1404.

10. Z. Li, X. Sun, X. Zheng, B. Li, D. Gao, S. Zhang, X. Wu, S. Li, J. Gong, J. M. Luther, Z. Li and Z. Zhu, *Science* 2023, **382**, 284-289.
11. H. Tang, Z. Shen, Y. Shen, G. Yan, Y. Wang, Q. Han and L. Han, *Science* 2024, **383**, 1236-1240.
12. J. Li, H. Liang, C. Xiao, X. Jia, R. Guo, J. Chen, X. Guo, R. Luo, X. Wang, M. Li, M. Rossier, A. Hauser, F. Linardi, E. Alvianto, S. Liu, J. Feng and Yi Hou, *Nature Energy* 2024, **9**, 308-315.
13. H. Zhang, S. Zhang, X. Ji, J. He, H. Guo, S. Wang, W. Wu, W.-H. Zhu and Y. Wu, *Angew. Chem. Int. Ed.* 2024, **63**, e202401260.
14. R. Azmi, D. S. Utomo, B. Vishal, S. Zhumagali, P. Dally, A. M. Risqi, A. Prasetio, E. Ugur, F. Cao, I. F. Imran, A. A. Said, A. R. Pininti, A. S. Subbiah, E. Aydin, C. Xiao, S. I. Seok and S. D. Wolf, *Nature* 2024, **628**, 93-98.
15. Y. Zheng, Y. Li, R. Zhuang, X. Wu, C. Tian, A. Sun, C. Chen, Y. Guo, Y. Hua, K. Meng, K. Wu and C.-C. Chen, *Energy Environ. Sci.* 2024, **17**, 1153-1162.
16. J. Zhou, L. Tan, Yue Li, H. Li, X. Liu, M. Li, S. Wang, Y. Zhang, C. Jiang, R. Hua, W. Tress, S. Meloni and C. Yi, *Joule* 2024, **8**, 1691-1706.
17. X. Hu, N. Shen, D. Zhang, Y. Wu, R. Shang, L. Wang and C. Qi, Adv. Mater. 2024, **36**, 2313099.
18. Z. Yi, W. Wang, R. He, J. Zhu, W. Jiao, Y. Luo, Y. Xu, Y. Wang, Z. Zeng, K. Wei, J. Zhang, S.-W. Tsang, C. Chen, W. Tangm and D. Zhao, *Energy Environ. Sci.* 2024, **17**, 202-209.
19. T. Duan, S. You, M. Chen, W. Yu, Y. Li, P. Guo, J. J. Berry, J. M. Luther, K. Zhu and Y. Zhou, *Science* 2024, **384**, 878-884.
20. S. Liu, J. Li, W. Xiao, R. Chen, Z. Sun, Y. Zhang, X. Lei, S. Hu, M. Kober-Czerny, J. Wang, F. Ren, Q. Zhou, H. Raza, Y. Gao, Y. Ji, S. Li, H. Li, L. Qiu, W. Huang, Y. Zhao, B. Xu, Z. Liu, H. J. Snaith, N.-G. Park and W. Chen, *Nature* 2024, **632**, 536-542.
21. Y. Shen, T. Zhang, G. Xu, J. A. Steele, X. Chen, W. Chen, G. Zheng, J. Li, B. Guo, H. Yang, Y. Wu, X. Lin, T. Alshahrani, W. Yin, J. Zhu, F. Wang, A. Amassian, X.

Gao, X. Zhang, F. Gao, Y. Li and Y. Li, Nature 2024, **635**, 882–889.

22. S. Li, Y. Xiao, R. Su, W. Xu, D. Luo, P. Huang, L. Dai, P. Chen, P. Caprioglio, K. A. Elmestekawy, M. Dubajic, C. Chosy, J. Hu, I. Habib, A. Dasgupta, D. Guo, Y. Boeije, S. J. Zelewski, Z. Lu, T. Huang, Q. Li, J. Wang, H. Yan, H.-H. Chen, C. Li, B. A. I. Lewis, D. Wang, J. Wu, L. Zhao, B. Han, J. Wang, L. M. Herz, J. R. Durrant, K. S. Novoselov, Z.-H. Lu, Q. Gong, S. D. Stranks, H. J. Snaith and R. Zhu, *Nature* 2024, **635**, 874-881.
23. Z. Liang, Y. Zhang, H. Xu, W. Chen, B. Liu, J. Zhang, H. Zhang, Z. Wang, D.-H. Kang, J. Zeng, X. Gao, Q. Wang, H. Hu, H. Zhou, X. Cai, X. Tian, P. Reiss, B. Xu, T. Kirchartz, Z. Xiao, S. Dai, N.-G. Park, J. Ye and X. Pan, *Nature* 2023, **624**, 557-563.
24. S. M. Park, M. Wei, N. Lempesis, W. Yu, T. Hossain, L. Agosta, V. Carnevali, H. R. Atapattu, P. Serles, F. T. Eickemeyer, H. Shin, M. Vafaie, D. Choi, K. Darabi, E. D. Jung, Y. Yang, D. B. Kim, S. M. Zakeeruddin, B. Chen, A. Amassian, T. Filleter, M. G. Kanatzidis, K. R. Graham, L. Xiao and E. H. Sargent, *Nature* 2023, **624**, 289-294.
25. Z. Huang, Y. Bai, X. Huang, J. Li, Y. Wu, Y. Chen, K. Li, X. Niu, N. Li, G. Liu, Y. Zhang, H. Zai, Q. Chen, T. Lei, L. Wang and H. Zhou, *Nature* 2023, **623**, 531-537.
26. Z. Qu, Y. Zhao, F. Ma, L. Mei, X.-K. Chen, H. Zhou, X. Chu, Y. Yang, Q. Jiang, X. Zhang and J. You, *Nat. Commun.* 2024, **15**, 8620.
27. Q. Li, H. Liu, C.-H. Hou, H. Yan, S. Li, P. Chen, H. Xu, W.-Y. Yu, Y. Zhao, Y. Sui, Q. Zhong, Y. Ji, J.-J. Shyue, S. Jia, B. Yang, P. Tang, Q. Gong, L. Zhao and R. Zhu, *Nature Energy* 2024, **9**, 1506-1516.
28. Y. Huang, K. Yan, X. Wang, B. Li, B. Niu, M. Yan, Z. Shen, K. Zhou, Y. Fang, X. Yu, H. Chen, L. Zhang and C.-Z. Li, *Adv. Mater.* 2024, **36**, 2408101.
29. M. Tao, Yang W., K. Zhang, Z. Song, Y. Lan, H. Guo, L. Guo, X. Zhang, J. Wei, D. Cao and Y. Song, *Joule* 2024, **8**, 1-11.
30. J. Du, J. Chen, B. Ouyang, A. Sun, C. Tian, R. Zhuang, C. Chen, S. Liu, Q. Chen, Z. Li, X. Wu, J. Cai, Y. Zhao, R. Li, T. Xue, T. Cen, K. Zhao and C.-C. Chen,

Energy Environ. Sci., 2025, doi.org/10.1039/D4EE05849F.

31. Z. Qin, M. Chen, Z Zhang, Y. Wang and L. Han, *Energy Environ. Sci.*, 2025, doi.org/10.1039/D4EE05968A.